Carbon nanotubes, buckyballs, ropes, and a universal graphitic potential

L. A. Girifalco, Miroslav Hodak, and Roland S. Lee*
Department of Material Science and Engineering, University of Pennsylvania, Philadelphia, Pennsylvania 19104
(Received 20 June 2000)

The potential energies of interaction between two parallel, infinitely long carbon nanotubes of the same diameter, and between C_{60} and a nanotube in various arrangements, were computed by assuming a continuous distribution of atoms on the tube and ball surfaces and using a Lennard-Jones (LJ) carbon-carbon potential. The constants in the LJ potential are different for graphene-graphene and C_{60}-C_{60} interactions. From these, the constants for tube-C_{60} interactions were estimated using averaging rules from the theory of dispersion forces. For tubes in ropes, the cohesive energy per unit length, the compressibility, and the equilibrium separation distance were computed as a function of tube radius. For a C_{60} molecule interacting with tubes, the binding energy inside a tube was much higher than on a tube or at the tube mouth. Within a tube, the binding energy was highest at a spherically capped end. The potential energies for tubes of all radii, as well as for interactions between C_{60} molecules, for a C_{60} molecule outside of a nanotube, between a C_{60} molecule and a graphene sheet, and between graphene sheets, all fell on the same curve when plotted in terms of certain reduced parameters. Because of this, all the potentials can be represented by a simple analytic form, thereby greatly simplifying all computations of van der Waals interactions in graphitic systems. Binding-energy results were all consistent with the recently proposed mechanism of peapod formation based on transmission electron microscopy experiments.

I. INTRODUCTION AND BACKGROUND

The Lennard-Jones (LJ) potential for two atoms a distance x apart is

$$u(x) = -\frac{A}{x^6} + \frac{B}{x^{12}}, \tag{1}$$

or, equivalently

$$u(x) = 4\epsilon\left[-\left(\frac{\sigma}{x}\right)^6 + \left(\frac{\sigma}{x}\right)^{12}\right]. \tag{2}$$

The equilibrium distance x_0 is given by

$$x_0 = 2^{1/6}\sigma = \left(\frac{2B}{A}\right)^{1/6} \tag{3}$$

and the well depth ϵ is

$$\epsilon = \frac{A^2}{4B}, \tag{4}$$

A and B being the attractive and repulsive constants in the Lennard-Jones potential.

Because of the clear separation of covalent and physical binding in graphitic solids, simple models based on this potential can describe those cohesive properties of such solids that depend on van der Waals interactions. These models have been widely used. A calculation of the interlayer cohesive properties of graphite successfully accounted for the energy of interlayer cohesion and c-axis compressibility of graphite using lattice sums of the LJ potential centered on atomic sites.[1] In a calculation of the molecular properties of C_{60} the model was simplified by treating the molecules as if they were perfect spheres and averaging the potential over their surfaces.[2]

This continuum model was also applied to a calculation of the thermal expansion[3] of solid C_{60}, to the cohesive and anharmonic properties[4] of solid C_{70}, and to fullerene alloys.[5,6] It was also used to analyze the growth of fullerene clusters,[7,8] screw dislocations[9] in solid C_{60}, the interaction of C_{60} with a graphite surface in which graphene sheets, as well as C_{60} molecules, were treated as surfaces with a uniform distribution of centers of the LJ potential[10] and to a study of C_{60} stage-one intercalated graphite.[11] Recently, the continuum model has been extended to a calculation of the potential between carbon nanotubes[12] and used to study the vibrational modes in nanotube bundles.[13] For C_{60}-C_{60}, graphene-graphene, and C_{60}-graphene interactions, the continuum model yielded potentials in terms of simple analytic functions. For interactions involving tubes this is not the case. The LJ interaction of a point with a continuous cylinder can be written in terms of the hypergeometric function[13] but even this simplification is lost when averaging over another surface and the potential contains integrals which must be evaluated numerically.

The true potential must recognize the correct charge distribution and the relative orientations of the interacting molecules. Several attempts to account for this have been made in which the molecule was treated as having discrete point charges at points on the molecular surface other than at atomic sites.[14–16] These ''bond charge'' models were not successful in reproducing the structural details of solid C_{60}. To remedy this, a model was introduced,[17] in which the potential was required to have the full symmetry of the molecule, using an electron distribution obtained from a local-density approximation to compute distributed Coulomb and

LJ interactions. This model gave reasonable agreement with experiment for both the high- and low-temperature phases.

Because of its simplicity, the continuum LJ model has been widely used. It has been shown to be quite successful in describing those cohesive properties of graphitic systems that are not sensitive to the details of orientational structure or the covalent binding. These properties include the molecular cohesive energy (which we define to be the energy required to separate the physically interacting graphitic structures without breaking covalent bonds), the lattice spacing, compressibility, thermal expansion, and equation of state, and the molecular contribution to the lattice vibrations and specific heat. They do not include such properties as librational spectra or the most stable orientational configurations of interacting graphitic structures which depend on the precise symmetry of the electron distribution.

One reason for the utility of the continuum LJ model is that there are instances in which the effect of the correct electron distribution is not important. An example of this is the C_{60} molecule at temperatures high enough that the molecules are rotating so that the instantaneous nonspherical distribution averages out to a spherical distribution. Another example is in carbon nanotube ropes in which the tube-tube interactions are an average over an ensemble of nanotubes of different chiralities and different relative orientations. Another reason is that some experimental results are used to compute the disposable parameters in the model, which is then applied to an analysis of other properties. Fixing the potential near the equilibrium position with experimental data gives good results for other properties that also depend on the potential near its minimum.

From a physical point of view, the discrete atom-atom model is not necessarily preferable to a continuum model. The discrete model assumes that each atom is the center of a spherically symmetric electron distribution while the continuum model assumes that the electron distribution is uniform over the surface. Both these assumptions are incorrect and a case can even be made that the continuum model is closer to reality than a set of discrete LJ centers.

The properties of ropes consisting of single walled carbon nanotubes have been investigated theoretically using a variety of methods.[18–20] The recent discovery of peapods[21] (which consist of C_{60} molecules encapsulated in carbon nanotubes) lends added importance to analyses of the interaction energies among tubes and C_{60}. In this paper, we extend the analysis of the continuum model to interactions in systems that include nanotubes and C_{60} molecules and we use the model to compute the properties of ropes.

Also, we show that potential energies of interactions for the continuum model for many graphitic structures fall on the same universal energy curve when plotted in terms of certain reduced parameters, thereby avoiding the need for numerical integrations in any future work.

There is an important point concerning which values of the LJ parameters to choose for the various systems. The constants for the graphite system differ substantially from those for the C_{60} system while each set of constants gives good results for the systems for which they were computed. Also, calculations using the continuum and the discrete approximations give similar results (see below) so the differences between the graphite system and the C_{60} system are not primarily the result of using a continuum rather than a discrete model. It seems clear that in systems with resonance π binding the constants obtained for graphite are preferable while in bucky balls, those derived from solid C_{60} data should be used.

TABLE I. Lennard-Jones constants in graphitic systems.

	A (eV×Å^6)	B (eV×Å^{12})	x_0 (Å)	$\lvert\epsilon\rvert$ (meV)
Graphene-graphene	15.2	24.1×10^3	3.83	2.39
C_{60}-C_{60}	20.0	34.8×10^3	3.89	2.86
C_{60}-graphene	17.4	29.0×10^3	3.86	2.62

However, many systems of interest include both π bond structures and fullerenes. For the interaction of unlike atoms, the constants can be computed from the approximations that the attractive constant and the equilibrium distance between atoms for two unlike molecules are the geometric and arithmetic mean, respectively.[22] Thus

$$A_{bg}=\sqrt{A_bA_g},\quad x_0^{bg}=\frac{x_0^b+x_0^g}{2}. \tag{5}$$

The label bg refers to the interaction of atoms in a C_{60} molecule with atoms in graphene or nanotubes, while the labels b and g refer to the interaction between atoms in C_{60} molecules and between atoms in graphene or nanotubes, respectively.

The values of interatomic Lennard-Jones constants for atoms in graphene-graphene, C_{60}-C_{60}, and C_{60}-graphene are shown in Table I.

Only the lattice parameter of graphite was used in computing the constants for the interactions in graphite; the attractive constant A_g was computed by Kraus.[23] The excellent agreement of the graphite calculations with experiment using these constants is probably fortuitous. The Lennard-Jones parameters for the interaction in solid C_{60} were computed by matching the calculated values of the cohesive energy and lattice constant to experimental data[2] and those for the C_{60}-graphene potential were computed from Eq. (5).

We note that in Eq. (3), although the well depth and the equilibrium distance are related, the equilibrium distance is a rather insensitive function of the original constants A and B in the LJ potential because it varies as the sixth root of their ratio. The difference between equilibrium distances for the atom-atom interactions for the graphite-based and C_{60}-based potentials is less than 2%. This difference is small because the repulsive part of the potential is very steep and its differences for the three potentials has only a small effect on computed properties since these depend primarily on the form of the potential near the equilibrium distance.

II. TUBE-TUBE INTERACTION POTENTIAL

In the continuum model the potential between two identical, parallel tubes is

$$\phi(R)=n_\sigma^2\int u(x)d\Sigma_1d\Sigma_2, \tag{6}$$

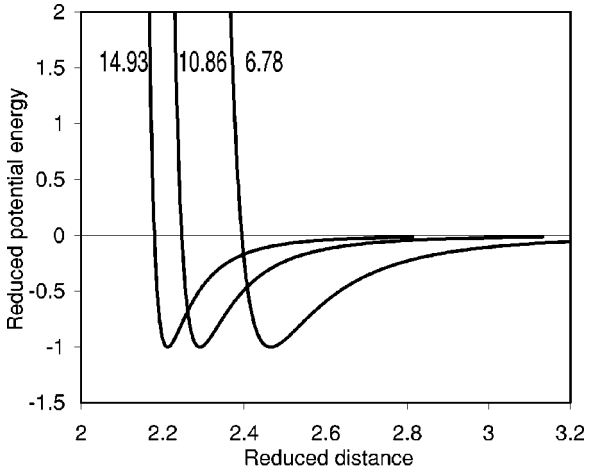

FIG. 1. Tube-tube interaction potentials for three different radii in units of the well depth and the ratio of distance to tube radius.

where n_σ is the mean surface density of carbon atoms and x is the distance between two surface elements $d\Sigma_1$ and $d\Sigma_2$ on two different tubes. The surface integral can be simplified to give

$$\phi(R)=\frac{3\pi n_\sigma^2}{8r^3}\left(-AI_A+\frac{21B}{32r^6}I_B\right), \tag{7}$$

where R is the perpendicular distance between tube centers, $\phi(R)$ is the potential energy of interaction per unit length, and

$$I_A=\int[(\cos\theta_2-\cos\theta_1)^2 + (\sin\theta_2-\sin\theta_1+R')^2]^{-5/2}d\theta_1 d\theta_2, \tag{8}$$

$$I_B=\int[(\cos\theta_2-\cos\theta_1)^2 + (\sin\theta_2-\sin\theta_1+R')^2]^{-11/2}d\theta_1 d\theta_2, \tag{9}$$

with $R'=R/r$. Both variables in these integrals range from 0 to 2π.

The integrals are independent of the tube radius and need to be evaluated only once as a function of R' to be used in Eq. (7). They assume that the tubes are perfectly cylindrical and of infinite extent. The results therefore apply to tubes without faceting, and long enough that end effects can be neglected.

The potentials were computed for tubes of the type (n,n), where n ranges from 4 to 29 and are shown for three different tube radii in Fig. 1. As expected, the potential has a longer range, and the energy minimum occurs at a higher separation distance (in units of the tube diameter), the smaller the tube diameter. The repulsive component of the potential is close to that of a hard core model.

III. BALL-TUBE INTERACTION POTENTIALS

The interaction between a C_{60} molecule and a tube in the continuum approximation is obtained by averaging over the surface of each entity. Performing the average of the LJ potential over the sphere first, gives the potential between a tube and a C_{60} molecule as

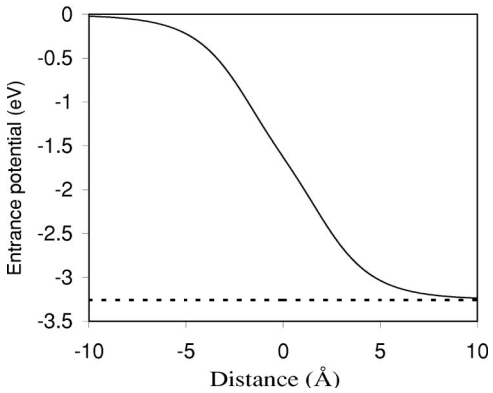

FIG. 2. The entrance potential for a C_{60} molecule near the open end of a (10,10) nanotube.

$$\phi_{bt}(l)=2\pi a n_\sigma^2\int\left[-\frac{A}{4}\left(\frac{1}{d(d-a)^4}-\frac{1}{d(d+a)^4}\right) + \frac{B}{10}\left(\frac{1}{d(d-a)^{10}}-\frac{1}{d(d+a)^{10}}\right)\right]d\Sigma_t, \tag{10}$$

where d is the distance of the tube surface element $d\Sigma_t$ from the center of the ball, l is the perpendicular distance between the axis of the cylinder and the center of the sphere, and a is the radius of C_{60} molecule. The integration over the tube depends on the configuration and tube radius under consideration.

Numerical integration of Eq. (10) is most easily done in cylindrical coordinates (r,φ,z), z being taken along the tube axis. If the C_{60} molecule is outside the nanotube, then $d=\sqrt{r^2+l^2+z^2-2rl\cos\varphi}$, where variable r is equal to the tube radius. If the C_{60} molecule is on the tube axis, then $d=\sqrt{r^2+z^2}$. This latter expression is valid for both finite and infinite tubes—only the range of integration is changed in Eq. (10).

For an infinite (10,10) tube, in which the C_{60} molecule is on the tube axis, the potential is independent of z and the calculation yields the binding energy of the molecule inside

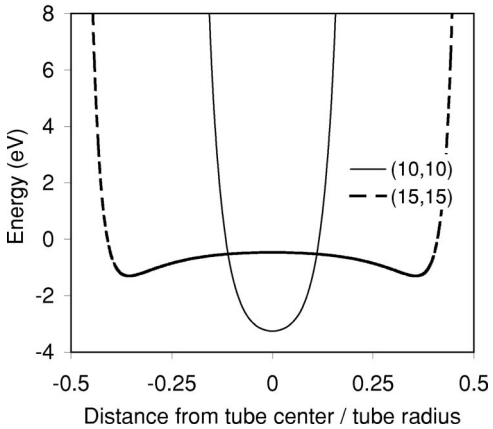

FIG. 3. The interaction potential of a C_{60} molecule inside a (10,10) and a (15,15) nanotube versus distance of C_{60} molecule from the tube center measured in nanotube radius units.

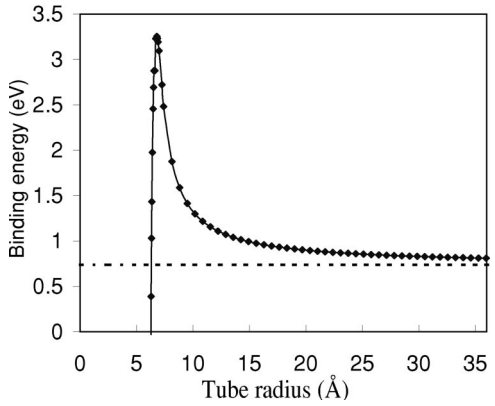

FIG. 4. The binding energy of a C_{60} molecule to the inside wall of a nanotube as a function of tube radius.

the tube. For a semi-infinite (10,10) tube in which the molecule is on the tube axis, but may be either inside or outside the open end of the tube, the calculation yields the potential energy as a function of distance as it enters the tube. We call this the entrance potential and it is shown in Fig. 2. Note that at a distance of 10 Å into the tube, the cohesive energy is very close to that of a C_{60} molecule in an infinite tube.

It is of interest to compute the binding energy of C_{60} to a spherical cap in a closed (10,10) tube. This is done by averaging over the cylinder and over the capping hemisphere.

The above ball-tube calculations are for a C_{60} molecule with a (10,10) tube so the interaction of the molecule with the tube is radially symmetric with a minimum at the tube axis. A number of calculations were made of the interaction of the C_{60} molecule with tubes of greater radii as a function of the radial distance from the tube axis. As expected, these showed that the potential had a minimum at the tube wall with a maximum at the tube center. Our calculations show that this is the case for tubes with radii higher than 7.3 Å. This is shown in Fig. 3 for a (10,10) and a (15,15) tube.

Figure 4 displays the binding energy of a C_{60} molecule at a tube wall as a function of tube radius. The curve has a maximum at 6.781 Å, which is almost exactly the radius of the (10,10) tube. Note that as the tube radius increases, the binding energy decreases and approaches the value for binding to a graphene sheet.

IV. THE UNIVERSAL GRAPHITIC POTENTIAL

The numerical integrations for the potential energy of interaction between two infinitely long tubes of the same radius, and between an infinitely long (10,10) tube with a molecule outside of the tube, showed that if the energy is

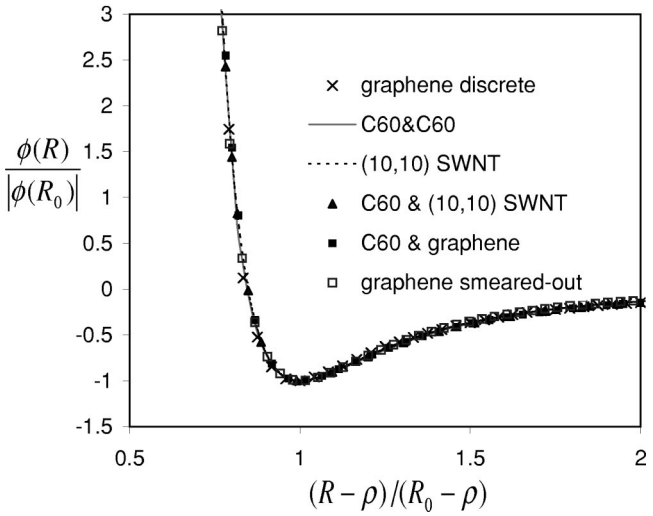

FIG. 5. The universal potential for graphitic structures.

expressed in units of the well depth, and the distance in terms of a reduced parameter, all potential plots fell on the same curve. That is, a plot of $\tilde{\phi} \equiv \phi(R)/|\phi(R_0)|$ against $\tilde{R} \equiv (R-\varrho)/(R_0-\varrho)$ gave the same curve for all tube-tube interactions and for interactions of a ball located outside an infinite (10,10) tube. R_0 is the equilibrium spacing at the minimum energy for the two interacting entities. If ϱ is the sum of the radii of the interacting objects than the definition of units above is natural: All the curves have a minimum equal to -1 at $\tilde{R}=1$ and the potential energy goes to infinity as the the distance approaches the sum of their radii because then the atoms on the considered objects start to overlap. However, in some systems a ϱ that is somewhat different than the sum of the radii must be used to fit the universal curve precisely.

For tube-tube interactions, $\varrho = 2r$, the diameter of the tube, gives excellent results. For the tube-ball interaction, taking ϱ to be the sum of the tube radius and the C_{60} radius, $\varrho = 10.33$ Å gives a reasonably good fit to the numerically computed curve, but decreasing this to $\varrho = 10.12$ Å improved the fit considerably.

This result can be generalized to include potentials between two graphene sheets, between two C_{60} molecules, and between a graphene sheet and a C_{60} molecule. Figure 5 shows that the superposition of the reduced potential for the various systems is very close and that a universal potential exists for these graphitic structures. The values that gave the best fit to the universal potential are given in Table II for the various interactions, except for the tube-tube interactions. For tube-tube interactions, the values of ϱ are just the tube

TABLE II. Energy and distance constants for the reduced parameters of the universal graphitic potential.

System	Distance parameter ϱ (Å)	Well depth $\lvert\phi(R_0)\rvert$	Equilibrium spacing R_0 (Å)
Graphene-graphene	0.28	15.36 meV/Å^2	3.414
Ball-ball	7.10	0.278 eV	10.05
Ball-(10,10) tube	10.12	0.537 eV	13.28
Ball-graphene	3.25	0.738 eV	6.508
(10,10) tube-(10,10) tube	13.57	95.16 meV/Å	16.724

TABLE III. Properties of ropes.

Tube type	Radius (Å)	Equilibrium spacing (Å)	Cohesive energy (eV/Å)	Bulk modulus (eV/Å^3)
(4,4)	2.714	8.550	−0.1793	0.1827
(6,6)	4.071	11.281	−0.2201	0.2198
(8,8)	5.428	14.004	−0.2547	0.2514
(10,10)	6.785	16.723	−0.2855	0.2808
(12,12)	8.142	19.441	−0.3136	0.3073
(14,14)	9.499	22.157	−0.3396	0.3318
(16,16)	10.856	24.873	−0.3639	0.3568
(18,18)	12.213	27.588	−0.3869	0.3764
(20,20)	13.570	30.303	−0.4085	0.3969
(22,22)	14.927	33.018	−0.4292	0.4163
(24,24)	16.283	35.733	−0.4490	0.4350
(26,26)	17.640	38.447	−0.4679	0.4529
(28,28)	18.997	41.162	−0.4862	0.4701

diameters that are obtained from Table III.

In Fig. 5, the curves for the graphene-graphene and tube-tube interactions were computed using the Lennard-Jones parameters fitted to the properties of graphite, the curve for the C_{60}-C_{60} interaction used the constants from the continuum model C_{60} study, while the constants used to get the C_{60}-tube, and C_{60}-graphene interactions were obtained from the averaging rules.

Results for graphite show that there is not much difference between the discrete atom and the continuum models when the same LJ parameters are used. In fact, calculations from the continuum model[11] gives -334 erg/cm^2 for the cleavage energy and 3.0×10^{-12} cm^2/dyn for the c axis compressibility while the corresponding numbers from the discrete calculation[1] are -330 erg/cm^2 and 3.18×10^{-12} cm^2/dyn. Song and Cappelletti[11] reported a cohesive energy value which they claimed was over 18% higher than that of Girifalco and Lad.[1] However, the number computed from the discrete calculation was for cleavage energy, not the total cohesive energy of separating graphite into planes an infinite distance apart, which is higher than the cleavage energy. The conclusion is that the discrete and continuum models give nearly the same results if the same LJ parameters are used.

The superposition of the potentials when expressed in terms of the reduced parameters allows us to write an analytic equation for all the continuum model potentials, including the tube-tube potentials, since it is also valid for the graphene-graphene, ball-ball, and ball-graphene potentials, all of which have simple analytic forms. Any of these can be chosen to give an analytic representation of the universal potential. Because it is the simplest, we choose the graphene-graphene potential which, per unit area of interacting sheets, is

$$\phi(R)=-\frac{2\pi n_\sigma^2 A}{4R_0^4}\left[\left(\frac{R_0}{R}\right)^4-0.4\left(\frac{R_0}{R}\right)^{10}\right], \tag{11}$$

or, dividing through by the well depth $|\phi(R_0)|$,

$$\frac{\phi(R)}{|\phi(R_0)|}=-\frac{1}{0.6}\left[\left(\frac{R_0}{R}\right)^4-0.4\left(\frac{R_0}{R}\right)^{10}\right], \tag{12}$$

the prefactor 0.6 being necessary to ensure that the reduced potential equals -1 at its minimum. Equation (12) is readily expressed in terms of the reduced parameter $\tilde{R}$ since, from its definition, the distance in the graphene-graphene potential is

$$R=\tilde{R}(R_0-\varrho)+\varrho=3.13\tilde{R}+0.28, \tag{13}$$

the numbers being taken from Table II for the graphene-graphene interaction, so that Eq. (12) is

$$\tilde{\phi}(\tilde{R})=\frac{\phi(R)}{|\phi(R_0)|}=-\frac{1}{0.6}\left[\left(\frac{3.41}{3.13\tilde{R}+0.28}\right)^4-0.4\left(\frac{3.41}{3.13\tilde{R}+0.28}\right)^{10}\right]. \tag{14}$$

This equation then gives the reduced potential for the systems listed in Table I when the appropriate values for R_0 and ϱ are used to compute the reduced distance.

The universal potential for graphitic structures is reminiscent of the universal energy curve of Rose *et al.*[24] However, the graphitic potentials could not be accurately represented by the equation of Rose *et al.* for the universal energy. This is not surprising since the graphitic potential is more anharmonic and much less symmetric about the minimum energy than the energy curve of Rose *et al.* Therefore the physical interpretation of the universal graphitic potential is different from that of Rose *et al.* Normalizing the energy by the well depth and the distance parameter by its value at equilibrium brings all curves into coincidence at the minimum energy and equilibrium distance just as for the curve of Rose *et al.* But the repulsive part of the graphitic potential is very steep and approximates a hard-sphere potential. It is therefore more accurate to correct the distance by hard-sphere radii than by a quasisymmetric deviation from harmonicity. That

this is not exact is shown by the fact that for unlike graphitic structures, the distance parameter is not quite the sum of the radii of the two structures.

V. PROPERTIES OF ROPES

The tube-tube interactions are negligible (less than 1% of the binding energy) at distances between centers that are twice the radius, so the ropes can be treated as if only the nearest neighbor were interacting. Table III shows the cohesive energy, the nearest-neighbor distance and the bulk modulus, all at the energy minimum, computed for ropes as a function of tube radius. These calculations refer to the rope properties that are parallel to the tube diameters.

The energy was well represented by the square-root fit

$$\phi_0(r) = -0.1135\sqrt{r} + 9.39\times 10^{-3}\ \text{eV/Å}, \qquad (15)$$

$\phi_0(r)$ being the energy of interaction in eV/Å at the minimum separation of parallel tubes each having a radius r in Angstroms.

The equilibrium distance R_0 at minimum energy varied linearly with radius according to the equation

$$R_0(r) = 2.00r + 3.13\ \text{Å}. \qquad (16)$$

Experimental data for the equilibrium distance is available for tubes with a diameter of 13.8 Å.[5] By minimizing our potential we get 16.95 Å, which is the same as the experimental result.

The best fit of the bulk modulus variation with radius according to the numbers in Table III is

$$B(r) = 0.106\sqrt{r} + 5.25\times 10^{-3}\ \text{meV/Å}^3. \qquad (17)$$

The bulk modulus increases less than three times as the tube radius is increased by a factor of 7. The reason for this is that for larger tubes, atoms on a tube surface are farther away from the atoms on the far side of the adjacent tube and see less of their attractive potential so the compressibility goes down. The compressibility of a rope was recently measured by Tang *et al.*[25] Their value is 0.024 GPa^{-1} for a rope of lattice constant 17.16 Å. Our theoretical calculation yields 0.022 GPa^{-1} for this rope.

The effect of intratube chemical bond energies has been ignored in this work. Calculations that include the valence forces[20] show that at tube diameters larger than 25 Å, the tubes in a rope become faceted and assume a quasihexagonal cross section. These calculations also show that as the diameter decreases, the tubes can be described by a model in which the van der Waals intertube interactions dominate. They found the same type of functional dependence for cohesive energy per Å, the bulk modulus, and equilibrium distance for radii below 25 Å.

A calculation of the elastic constants, equilibrium spacing, and cohesive energy has been performed by Lu[25] in which the intratube interaction was taken from a force constant model for graphite[26] and the intertube interaction was a sum of Lennard-Jones potentials with parameters chosen to fit the interlayer distance and elastic constants of graphite. He computed the same value as ours for equilibrium tube-tube separation for a rope of (10,10) nanotubes (16.7 Å). However, his value for the magnitude of the cohesive energy of ropes, 0.383 eV/Å was over 30% larger than our value of 0.285 eV/Å and his result for the bulk modulus was smaller than ours by a factor of 2 (0.280 eV/Å^3 versus 0.137 eV/Å^3). His calculation included the volume change arising from changes in covalent bond length, as well as from van der Waals interactions, but the effect of the intratube interaction should not be important for (10,10) tubes. Lu's result for bulk modulus is probably incorrect since in a similar paper Tersoff and Ruoff[20] computed 0.22 eV/Å^3, taking into account intratube covalent binding, but for a rigid cylinders they found a bulk modulus of 0.26 eV/Å^3. Their value for cohesive energy, 0.29 eV/Å, is in good agreement with ours.

VI. BINDING ENERGIES

We have computed the energy of interaction for two nanotubes per unit length. Considering the typical high length of nanotubes, the total van der Waals interaction between tubes becomes very strong. Because of this effect, the nanotubes in the samples will orient themselves to be parallel whenever possible, therefore forming crystalline ropes.

The binding energy of a ball inside a (10,10) tube is six times higher than the energy for C_{60} outside the tube. This is in accord with the existence of the recently discovered nanopeapods[21] which form easily and are quite stable.

Since the potential for entering the tube is highly attractive, any C_{60} molecule near the mouth of an open tube will be drawn into it. However, this potential is short-ranged (see Fig. 2), so the balls have to get into the nanotube mainly through defects in the tube wall. The formation mechanism can be described as follows: When an external ball in the gas phase gets close to the tube wall it forms a relatively stable configuration, since the binding energy to a tube is twice the interaction between C_{60} molecules. Once bound to an outer wall, a ball can slide relatively easily since the energy barrier for sliding is of the order of 0.1% of the binding energy to the wall,[27] until it finds a hole in the tube wall and eventually gets in. This is in accord with the mechanism of peapod formation proposed by Smith and Luzzi.[28]

Once the ball is inside the tube it can further increase its binding energy by interacting with the other internal balls or with a cap. The latter interaction is stronger. For a spherically capped (10,10) tube, the binding energy of a ball to the cap is 1.14 eV greater than the binding energy in an infinite tube. For nanotubes with large radii, the minimum of potential energy is shifted from its center to the walls. As a result, the regular distribution of bucky balls along the tube axis will disappear and balls will preferentially be found at the tube walls. For high concentrations, balls will also be found at other positions, provided the tube has a minimum diameter greater than about 31 Å, which is the sum of the effective diameters of three adjacent C_{60} molecules. This phenomenon was recently experimentally observed.[28]

The binding energies given in Table IV will be the major contribution to the free energies of formation. Assuming that the ordering of the free energies will be the same as that for the energies given in Table IV, it can be inferred that peapods are the most stable arrangement of C_{60} molecules in (10,10) tubes. It can also be concluded that intercalated C_{60} molecules, in which the balls are at interstitial positions be-

TABLE IV. Binding energies of a C_{60} molecule to a (10,10) tube.

System	Binding energy (eV)
Ball on top of a tube	0.537
Ball at the mouth of tube	1.63
Ball inside tube	3.26
Ball at a spherical cap	4.40

tween tubes in a rope, are probably less stable relative to the gas phase. The reason for this is that the cohesive energy of intercalated C_{60} molecule is -1.61 eV, whereas the corresponding cohesive energy for a rope of (10,10) tubes is 10.05 Å $x-0.2855$ eV/Å $=-2.87$ eV (10.05 Å is the effective diameter of a C_{60} molecule). This is physically reasonable since tube-tube interactions involve more atoms per unit length than tube-ball interactions.

VII. SUMMARY AND CONCLUSIONS

The van der Waals potential energy of interactions in graphitic structures was computed for various configurations of C_{60} molecules interacting with carbon single walled nanotubes, based on assuming a Lennard-Jones potential for the interaction between carbon atoms in the continuum model. It was found that, when the energy is expressed in units of the well depth and the distance in terms of a reduced parameter related to the diameters of the interacting entities, the tube-tube and ball-tube potentials all fell on the same curve. It was further found that the potential functions for graphene-graphene, ball-graphene, and C_{60}-C_{60} interactions also fell on the same curve when written in terms of the reduced parameters. The existence of this universal potential curve for graphitic structures allowed the potential functions to be written as a simple analytic form, thereby obviating the future need for extensive numerical calculation for tube-tube and ball-tube interactions.

The cohesive energy and bulk modulus of nanotubes consisting of ropes of the same diameter was each found to vary as the square root of the radius, while the equilibrium spacing was a linear function of radius. The entrance potential, which is the potential energy of a C_{60} molecule along the axis of an open (10,10) nanotube as a function of distance from the open end, was also computed.

For the interaction of a ball inside a tube, calculations were performed for the potential energy as a function of distance from the tube center with the expected result that for tube diameters larger than that for a (10,10) tube, the minimum energy was for a C_{60} molecule against the tube wall. The binding energy of a C_{60} molecule to the tube wall was computed as a function of tube radius. Binding energy was also computed for a bucky ball interacting with nanotubes in various configurations. All results were consistent with experiment.

ACKNOWLEDGMENTS

We gratefully acknowledge support for M.H. through the National Science Foundation Grant No. 98-02560 and for R.S.L. through the United States Department of Energy, DEFG 02-87ER45254 and DEFG 02-98ER45701.

*Present address: Laboratoire d'Etudes des Microstructures, 92322 Chatillon Cedex, France.

[1] L.A. Girifalco and R.A. Lad, J. Phys. Chem. **25**, 693 (1956).
[2] L.A. Girifalco, J. Phys. Chem. **96**, 858 (1992).
[3] L.A. Girifalco, Phys. Rev. B **52**, 9910 (1995).
[4] K. Kniaz, L.A. Girifalco, and J.E. Fischer, J. Phys. Chem. **99**, 16804 (1995).
[5] K. Kniaz, J.E. Fischer, L.A. Girifalco, A.R. McGhie, R.M. Strongin, and A.B. Smith, Solid State Commun. **96**, 739 (1995).
[6] V.I. Zubov, N.P. Tretiakov, J.N. Teixeira Rabelo, and J.F. Sanchez Ortiz, Phys. Lett. A **194**, 223 (1994).
[7] J.P.K. Doye and D. Wales, Chem. Phys. Lett. **247**, 339 (1995).
[8] J. Garcia-Rodeja, C. Rey, and L.J. Gallego, Phys. Rev. B **55**, 7190 (1997).
[9] S. Tamaki, N. Ide, I. Okada, and K. Kojima, J. Appl. Phys. **37**, 2608 (1998).
[10] R.S. Ruoff and A.P. Hickman, J. Phys. Chem. **97**, 2494 (1993).
[11] J. Song and R.L. Cappelletti, Phys. Rev. B **50**, 14 678 (1994).
[12] R.S. Lee and L.A. Girifalco (unpublished).
[13] L. Henrard, E. Hernandez, P. Bernier, and A. Rubio, Phys. Rev. B **60**, R8521 (1999).
[14] J.P. Lu, X.P. Li, and R.M. Martin, Phys. Rev. Lett. **68**, 1551 (1992).
[15] M. Sprik, A. Cheng, and M.L. Klein, J. Phys. Chem. **96**, 2027 (1992).
[16] E. Burgos, E. Halac, and H. Bonadeo, Phys. Rev. B **47**, 13 903 (1993).
[17] S. Savin, A.B. Harris, and T. Yildirim, Phys. Rev. B **55**, 14 182 (1997).
[18] J.C. Charlier, X. Gonze, and J.P. Michenaud, Europhys. Lett. **29**, 43 (1995).
[19] D. Sanchez-Portal, E. Artacho, and J.M. Soler, Phys. Rev. B **59**, 12 678 (1999).
[20] J. Tersoff and R.S. Ruoff, Phys. Rev. Lett. **73**, 676 (1994).
[21] B.W. Smith, M. Monthioux, and D.E. Luzzi, Nature (London) **396**, 3239 (1998); Chem. Phys. Lett. **315**, 31 (1999).
[22] For the background of this approximation based on theories of dispersion forces see, J. Hirschfelder, C.F. Curtis, and R.B. Bird, *Molecular Theory of Gases and Liquids* (Wiley, New York, 1954), Chap. 13.
[23] G. Kraus, University of Cincinnati, Progress Report No. 2, Army Air Force Contract AF33(616) (1953).
[24] J.H. Rose, J.R. Smith, F. Guinea, and J. Ferrante, Phys. Rev. B **29**, 2963 (1984).
[25] J.P. Lu, Phys. Rev. Lett. **79**, 1297 (1997); J. Tang, L. Qin, T. Sasaki, M. Yuclasaka, A. Matsushita, and S. Iijima, *ibid.* **85**, 1887 (2000).
[26] R. Al-Jishi and G. Dresselhaus, Phys. Rev. B **26**, 4514 (1982).
[27] M. Hodak and L.A. Girifalco (unpublished).
[28] B.W. Smith and D.E. Luzzi, Chem. Phys. Lett. **321**, 169 (2000).